OPTO-ELECTRONICS REVIEW **13**(2), 75–84

Wide beam stabilities and instabilities in one dimensional arrays of Kerr-nonlinear channel waveguides

J. MEIER*[1], D.N. CHRISTODOULIDES[1], G.I. STEGEMAN[1], H. YANG[2], G. SALAMO[2], R. MORANDOTTI[3], J.S. AITCHISON[4], and Y. SILBERBERG[5]

[1]College of Optics & Photonics: CREOL & FPCE, University of Central Florida, Orlando, FL 32816, USA
[2]Department of Physics, University of Arkansas, Fayetteville, AR 72701, USA
[3]Institut National de la Recherché Scientifique, University du Québec, Varennes, Québec, J3X 1S2, Canada
[4]Department of Electrical and Computer Eng., University of Toronto, Toronto, Ontario, M5S 3G4, Canada
[5]Department of Physics of Complex Systems, The Weizmann Institute of Science, 76100 Rehovot, Israel

The propagation of wide (plane-wave like) and narrow high intensity beams at 1550 nm was investigated in 1D arrays of AlGaAs channel waveguides which are nearest-neighbour coupled via evanescent fields. Spatial diffraction (beam spreading) by evanescent field coupling leads to dispersion relations that are periodic with propagation direction and hence exhibit regions of both normal and anomalous diffraction. This results in propagation directions in which filamentation of high intensity beams with superimposed noise occurs, and other regions in which these beams are stable against noise. Both cases were observed experimentally, and the modulation instability gain was measured versus the spatial frequency of the noise. Good agreement with theory was found.

Keywords: discrete nonlinear optics, modulation instability, solitons.

1. Introduction

One- and two-dimensional (1D and 2D, respectively) arrays of weakly coupled channel waveguides have many interesting properties unique to discreteness [1]. Light travels along the channels and can spread throughout the array via discrete diffraction. The evanescent tails of the individual channels overlap the neighbouring channels and light "leaks" from channel to channel [2]. For "plane waves", this results in periodic dispersion relations for the transverse (Bloch) wavevector in terms of the longitudinal propagation constant [1,3]. This in turn leads to ranges of propagation angles that exhibit "anomalous" as well as "normal" diffraction. This feature, the existence of "anomalous" diffraction, has interesting repercussions on nonlinear optics in discrete systems.

It has been well-known for many years now that spatial solitons and modulation instability (filamentation) are manifestations of the same physics in media with a self-focusing nonlinearity [4–6]. Spatial solitons, self-trapped beams, are formed when diffraction and self-focusing are balanced robustly. This occurs when a finite cross-section beam is incident in a self-focusing material with a peak intensity comparable to that required for self-trapping. However, if the beam at some intensity is much wider (quasi-plane wave) than required for a spatial soliton, noise on the beam envelope leads to filamentation (break-up) of the broad beam [7]. Because spatial solitons are the natural eigenmodes of high intensity beams in nonlinear media, each of these filaments evolves towards a spatial soliton if indeed solitons are stable in that geometry. Otherwise filaments are formed which continue to change shape and intensity during propagation. This latter case, for example, occurs in a bulk medium governed by a pure Kerr nonlinearity.

The transition between these two effects which depend on the trade-off between input power and beam width, soliton generation and modulational instability has been demonstrated using the cascading second order nonlinearity [8]. Both spatial solitons and modulational instability have been observed separately near the phase-matching condition for second harmonic generation by launching into the samples high intensity beams at the fundamental frequency [9]. By increasing the input intensity of a fundamental beam to well beyond the soliton threshold, the progression through single soliton generation, multiple soliton generation and then filamentation has been observed in $LiNbO_3$ slab waveguides (1D case) [8,10]. Dramatic differences in the nature of the filamentation would be expected for discrete systems because "anomalous" diffraction is allowed [11,12]. By analogy to the case of nonlinear temporal effects in fibers where temporal dispersion can be either normal or anomalous [13], and filamentation only occurs in the anomalous temporal dispersion regime, spatial filamentation should not occur in the anomalous diffraction regime.

*e-mail: jmeier@mail.ucf.edu

In this paper we describe nonlinear optics experiments with wide (10's of channels wide) and narrow (few channels wide) beams leading to stable propagation for some directions and filamentation for others. The experiments were performed in AlGaAs arrays which are known to exhibit almost ideal, self-focusing Kerr-law nonlinearities for photon energies just below one half the semiconductor bandgap. A short description of these experiments has already been published in literature [14].

2. Discrete diffraction in arrays

Consider a pair of identical, parallel channel waveguides, identified as "n" and "$n + 1$". The concept of beam coupling in an array of channels is rooted in the response of such a well-known directional coupler of integrated optics shown in Fig. 1 [15,16].

The evanescent field of channel waveguide n, $a_n(z)E(x)$ couples to an identical waveguide $n + 1$ which leads to a transfer of energy with the distance from n to $n + 1$. After "one-half beat length" L_C there is net energy flow back to n from $n + 1$. The equations which govern this exchange are

$$\begin{aligned} i\frac{d}{dz}a_{n-1}(z) + \beta a_{n-1}(z) + Ca_n(z) = 0 \\ \frac{d}{dz}a_n(z) + \beta a_n(z) + Ca_{n-1}(z) = 0 \end{aligned}, \qquad (1)$$

where β is the single isolated channel propagation wavevector and $C = \pi/(2L_C)$ is the coupling constant. For the n-th channel inside an array of many waveguides (Fig. 2), coupling can occur to both the neighbouring channels, $n - 1$ and $n + 1$ so that for each channel [2,17]

$$i\frac{d}{dz}a_n(z) + \beta a_n(z) + C(a_{n+1}(z) + a_{n-1}(z)) = 0. \qquad (2)$$

The discrete plane wave solutions (constant envelope field a_n) in 1D to these equations for the array are obtained by writing the n-th field as

$$a_n = E_0 \exp(i(nk_x d + k_z z)), \qquad (3)$$

where d is the centre-to-centre channel separation, k_x and k_z are the longitudinal (along z) and transverse (along x) wavevectors and $k_x d = \Delta\theta$ is the relative phase angle between the fields in adjacent channels. For the simulations presented later, a time-independent wave has been assumed. Substituting Eq. (3) into Eq. (2) gives the dispersion relation [3]

$$k_z = \beta + 2C\cos(k_x d). \qquad (4)$$

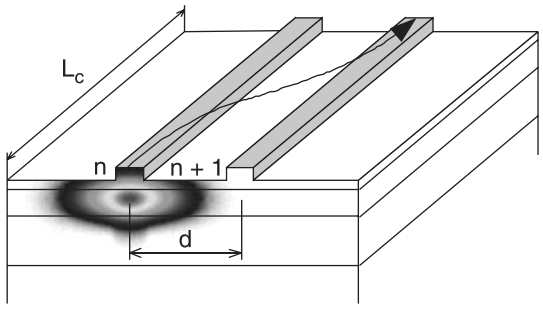

Fig. 1. Directional coupler.

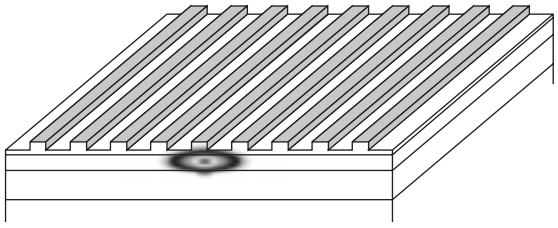

Fig. 2. Waveguide array.

This dispersion relation is plotted in Fig. 3. There is a maximum angle which occurs at $\Delta\theta = \pi/2$ at which the beam can "slide" across the array due to the evanescent coupling. Note also that excitation at $\Delta\theta = \pi$ results in light propagating straight along the array, with relative phase angle π between channels, the so-called "staggered" solution [11]. Further, the dispersion has a periodicity of $|k_x d| = 2\pi$. Therefore excitation at $\Delta\theta = 0$ or $\Delta\theta = 2\pi$ lead to identical propagation through the array.

In continuous media, the strength of diffraction depends on the curvature of the dispersion curve. Clearly from Fig. 4, "discrete" diffraction in the array varies with $\Delta\theta$. In analogy with dispersion in the temporal domain, diffraction can be quantified by

$$D = -\frac{d^2 k_z}{dk_x^2}, \qquad (5)$$

so that for the arrays $D = 2Cd^2\cos(k_x d)$. In the first "Brillouin" zone (i.e. $0 \le |k_x d| \le \pi$), normal diffraction (i.e., D is positive) occurs for $0 \le |k_x d| \le \pi/2$. However, for $\pi/2 \le |k_x d| \le \pi$, D is negative, i.e., the diffraction is "anomalous", a phenomenon nonexistent in homogeneous media. Note that at $|k_x d| = \pi/2$, the second order diffraction is zero, i.e., a beam can cross the array without spreading. But, narrow width beams do spread due to higher order

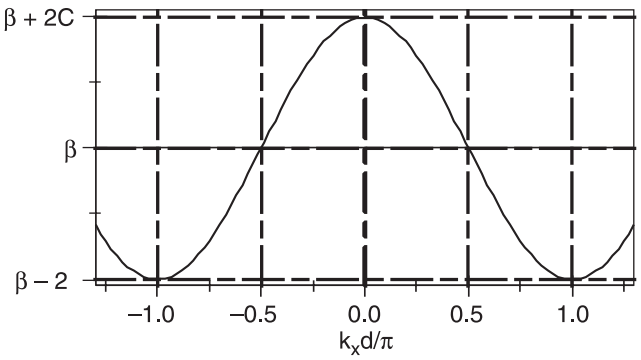

Fig. 3. Dispersion relation.

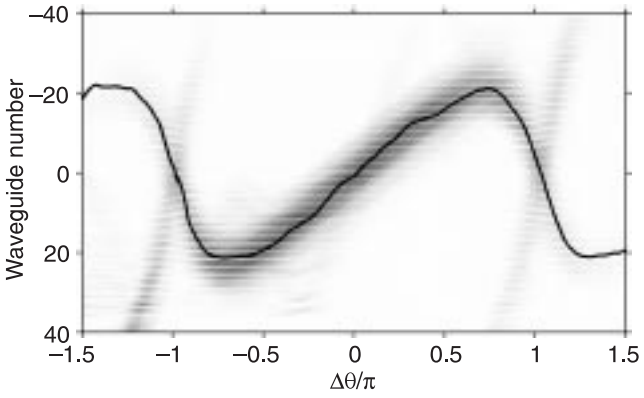

Fig. 4. Measured displacement on a tilted beam in an AlGaAs array. The black line shows the location of the beam centre.

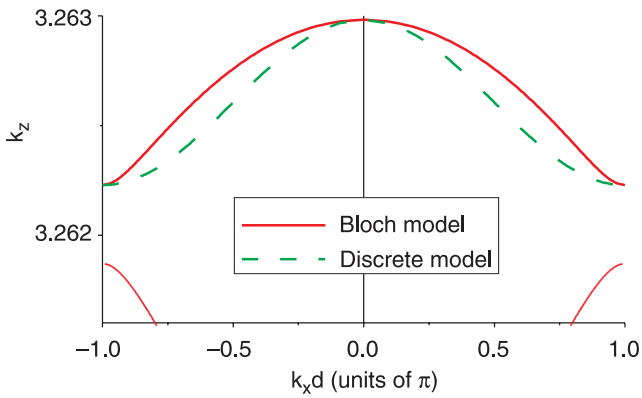

Fig. 5. The calculated lowest order band as obtained from the discrete couple mode theory (dashed line) and from the more accurate Bloch model (solid line).

diffraction effects since they contain a finite spectrum of $|k_x d|$ around $\pi/2$.

The dispersion relation described by Eq. (4) was investigated by propagating a wide beam down an array with variable phase angle $\Delta\theta$ between adjacent channels. (This was achieved by simply directing a planar wavefront onto the front facet of the sample at small angles relative to the channel axes.) The resulting beam follows the normal to the dispersion curve and is deflected away from the centre channel as the incidence angle is varied. The displacement Δx of the centre of the beam with incidence angle should follow $\Delta x = -2Cd\sin(dk_x)$ functional dependence [1,11,18]. The beam displacement was measured as a function of $\Delta\theta$ and a typical result is shown in Fig. 4. The deviation from the simple theory just presented is very clear.

The simple coupled wave picture presented here, although attractive for its simplicity, is just the lowest approximation to the modes supported by these periodic structures. In fact, it has been shown that an analysis of this structure into Floquet-Bloch modes yields in addition to the fundamental band just discussed a set of higher order bands neglected in the simple coupled mode theory presented. The result of such an analysis is shown in Fig. 5. Note that the point of inflection in the curvature occurs for $|k_x d| = 0.6\pi$. As a result, the anomalous diffraction region is smaller than predicted by coupled mode theory.

3. Modulational instability theory: coupled mode approach

This unique form of diffraction and dispersion described above, when combined with a self-focusing ($n_2 > 0$) nonlinearity, has some interesting repercussions to soliton physics, specifically in the realm of modulational instability. The coupled mode formalism is used in the small signal regime for convenience.

Consider a single polarization of light. Adding the Kerr nonlinearity to the coupled wave equations gives [3]

$$\begin{aligned} & i\frac{d}{dz}a_n(z) + \beta a_n(z) \\ & + C[a_{n+1}(z) + a_{n-1}(z)] + n_2 k_0 |a_n|^2 a_n = 0 \end{aligned} . \qquad (6)$$

As stated in the introduction, modulational instability and spatial solitons derive from the same nonlinear physics. For the single polarization case of interest here, Eq. (6) describes the evolution of nonlinear beams in the array. One now introduces a "noise" perturbation $\Delta_n(z)$ onto a 1D "plane wave" beam. The origin of this perturbation can be noise on the input optical beam, imperfections in the sample etc. and the perturbed beam due to a single spatial Fourier component of the noise can be written as [3,19]

$$a_n = (E_0 + \Delta_n(z))\exp(-ink_x d)\exp(-ik_z z). \qquad (7)$$

In turn, the spatial Fourier component of the noise perturbation can be written as

$$\begin{aligned} \Delta_n(z) = {} & \Delta_n^+ \exp(i(K_z z - nK_x d)) \\ & + \Delta_n^- \exp(-i(K_z z - nK_x d)) \end{aligned} . \qquad (8)$$

The field a_n is now substituted into Eq. (6), and using the fact that E_0 satisfies Eq. (2) by itself, two equations in terms of the small amplitudes Δ_n^+ and Δ_n^- can be derived. These equations can be solved for the dispersion relation between K_x and K_z giving [19]

$$K_z = \pm\sqrt{8c\cos(\Delta\theta)\sin^2\left(\frac{K_x d}{2}\right)\left[2C\cos(\Delta\theta)\sin^2\left(\frac{K_x d}{2}\right) - n_2 k_0 E_0^2\right]} + 2C\sin(\Delta\theta)\sin(K_x d). \qquad (9)$$

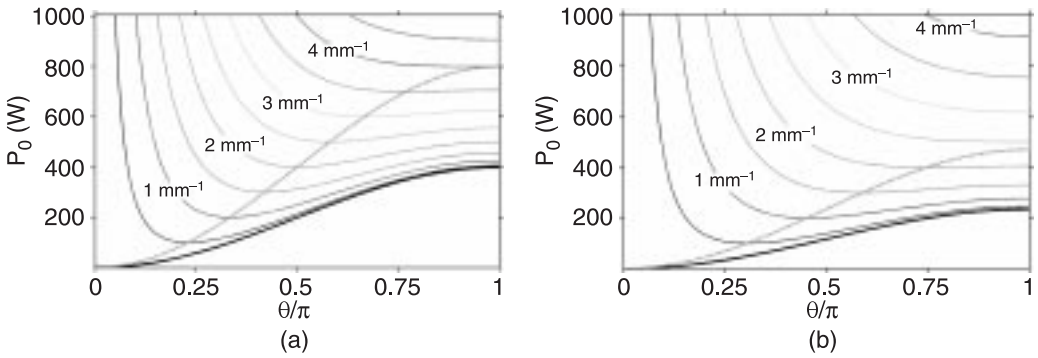

Fig. 6. Calculated MI gain for an AlGaAs sample with C = 1000 m^{-1} for (a) $\Delta\theta = 0$ and (b) $\Delta\theta = 0.3\pi$.

For the perturbation Fourier component to grow with the propagation distance z, K_z must be imaginary. This leads to the condition

$$\cos(\Delta\theta)\left[2C\cos(\Delta\theta)\sin^2\left(\frac{K_x d}{2}\right) - n_2 k_0 E_0^2\right] < 0, \quad (10)$$

which only occurs for $|k_x d| < \pi/2$, i.e., in the region of "normal" diffraction. Thus, filamentation can only occur for $|\Delta\theta| < \pi/2$. (For the actual mode dispersion, the onset of filamentation will occur for $|\Delta\theta| < 0.6\pi$). Note that there are also power thresholds for MI for a given Fourier component K_x, discussed in the next paragraph.

Just as in the case of 1D homogeneous Kerr media, analytic relations can be obtained for the threshold of the onset of modulational instability and the maximum gain. From Eq. (10), the threshold field for the appearance in MI is given by

$$E_0^2 \geq \frac{2}{k_0 n_2} C\cos(\Delta\theta)\sin^2\left(\frac{K_x d}{2}\right) \quad (11)$$

and the maximum gain is given by

$$(K_x d)_{\max} = \arccos\left[\frac{1}{2C}\sec(\Delta\theta)(2C\cos(\Delta\theta) - k_0 n_2 E_0^2)\right]. \quad (12)$$

Plotted in Fig. 6 is the variation in the gain coefficient with the relative phase shift $\Delta\theta$ between adjacent channels and the input power for 1D "plane wave" inputs. The power threshold (solid lines) decreases with increasing $\Delta\theta$. The maximum gain (dashed lines) increases with the power per channel P_0 and $\Delta\theta$. At the critical power $E_0^2 = 4C\cos(\Delta\theta)/(k_0 n_2)$ maximum gain only occurs at $\Delta\theta = \pi$.

4. AlGaAs array samples

The samples used in the experiments were AlGaAs slab waveguides into which individual, closely spaced channels were etched to form multiple arrays, typically each consisting of 101 waveguides. The planar structure was MBE deposited onto GaAs substrates and consisted of a 4-μm thick lower cladding region of $Al_{0.24}Ga_{0.76}As$, a 1.5-μm thick guiding layer of $Al_{0.18}Ga_{0.82}As$, and a 1.5-μm thick upper cladding region of $Al_{0.24}Ga_{0.76}As$. Array samples, shown in Fig. 7, with inter-channel coupling constants C of 0.8 mm^{-1} and 1.1 mm^{-1} were fabricated by judiciously choosing both the centre-to-center channel separation d (9 μm) and the etch depth e.

AlGaAs channel waveguides of this composition, singly and as directional couplers, have been studied previously for all-optical switching [20,21]. Towards that end, both the wavelength dependence of the real and imaginary components of the third order susceptibility were measured as a function of photon energy in the immediate vicinity of half the semiconductor's bandgap [22–24]. The results showed that for photon energies below one half of the bandgap, the nonlinear response was Kerr-like with minimal multi-photon absorption. Such previous characterization of the channel waveguides established the effective nonlinearity to be n_2 = 1.5 ×10^{-13} cm^2/W and linear propagation losses were found to be typically less than 1.5 dB/cm.

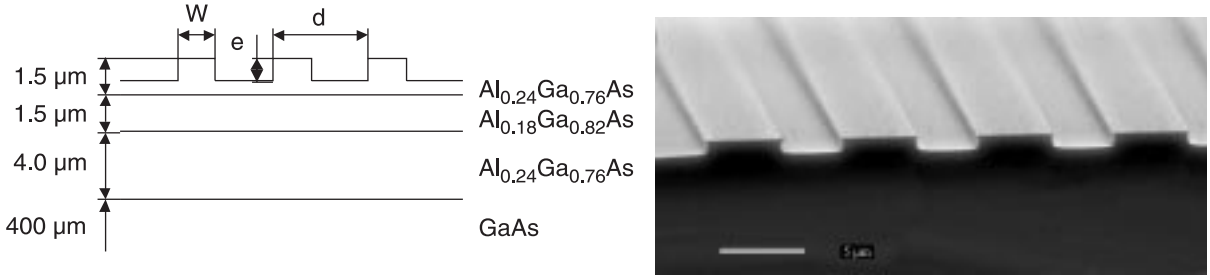

Fig. 7. Array structure and electron microscope image of an array.

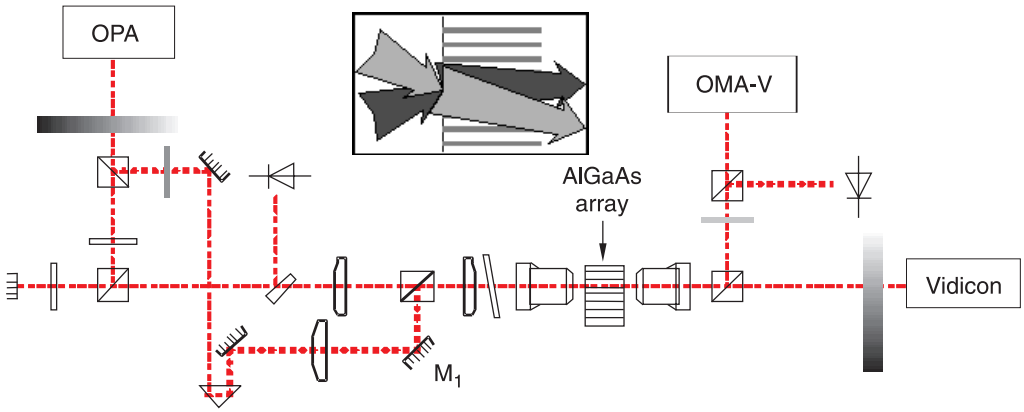

Fig. 8. Experimental setup. Shown in the inset are two incident coherent beams whose interference results in a periodic modulation of the more intense beam.

5. Experimental details

The experimental geometry is shown in Fig. 8. These experiments in their simplest form require a single wide elliptical input beam, and for the measurement of the MI gain an additional, co-polarized, wide, weak seed beam injected into the array at a variable angle to the strong pump beam to form an interference pattern with variable fringe spacing. The source was a tunable Spectra Physics OPA pumped by a Ti:sapphire laser which was amplified by a Ti:Sapphire regenerative amplifier. The system produced pulses between 1300 nm and 3000 nm of 1 ps duration at a 1 kHz repetition rate with individual pulses having energies up to 30 μJ around 1550 nm. The individual pulses were split by a beamsplitter cube into two co-polarized beams and temporally overlapped using delay lines.

For the first set of experiments only a single beam path was used. The required elliptical beam was formed by a combination of elliptical and circular lenses which were arranged to have a common focus for both beam dimensions at the input facet of the array. A parallel plate mounted on a rotation stage before the microscope objective was used for tilting the input beam direction (and hence varying $\Delta\theta$). The input and output beam powers were both measured by detectors. A vidicon camera was used to align the system and a linear Roper OMA-V InGaAs array was used to acquire data right down to very low power levels.

For the MI gain measurements, the set-up just described was used with minor modifications. The beam geometry into the sample is shown schematically in the inset of Fig. 8. A second beam path was introduced to produce a weak perturbation beam (amplitude 5% of the strong beam amplitude). Each beam is then transmitted through a common lens train and focused onto the array.

6. Modulational instability due to noise

A single 250 × 1.5 μm beam of variable power was first directed at varying angles of incidence onto the array's input facet of the 8 mm long sample. Figures 9(a)–(c) show the observed output patterns for input beam angles varying be-

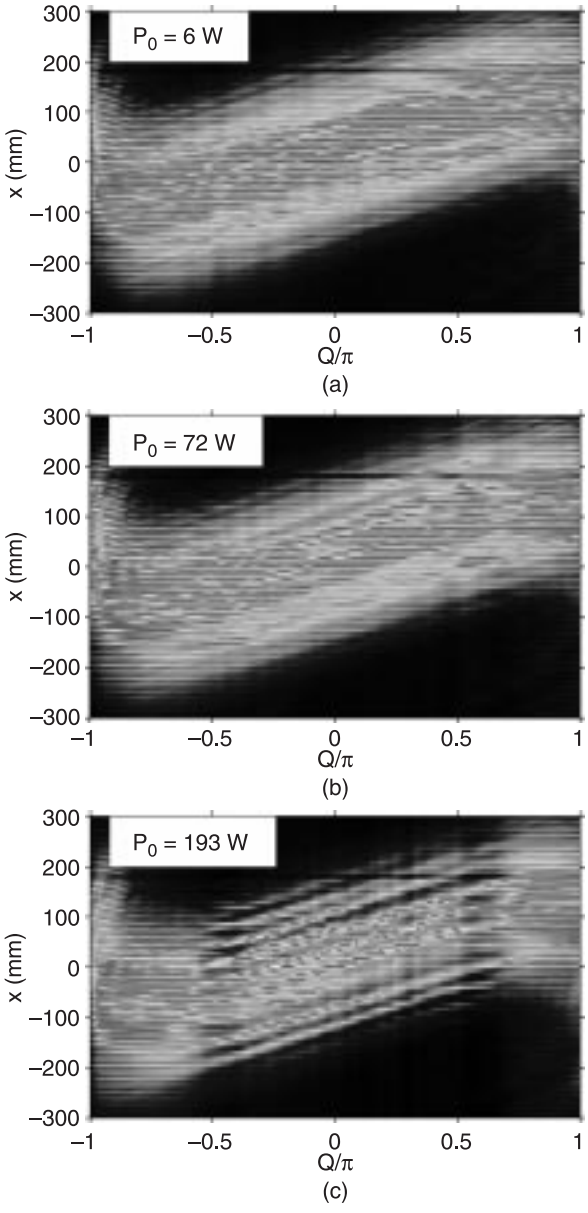

Fig. 9. Measured intensity distribution at the array output for (a) 6 W, (b) 72 W and (c) 193 W powers used to excite the central channel. $Q = \Delta\theta$ is the relative phase between adjacent channels.

tween $\pm\pi$ for three different power levels. The outputs move across the array due to the different transverse wavevectors associated with varying $\Delta\theta$. No modulation instability was observed [Fig. 9(a)] at the lowest power of 6 W (estimated peak power in the central waveguide). The "striations" observed are due to "noise" on the beam, probably due to imperfections on the input coupling facet. As the input power is increased for angles where the array exhibits normal diffraction, these distortions start to grow at the expense of the background power between them, whereas in the negative diffraction region the beam shows no sign of any instabilities. This behaviour is clear at intermediate powers of 72 W. With further increase in input power, this noise is further amplified in the anomalous dispersion regime resulting in large contrast striations or filaments. At the highest shown input power level of 193 W peak per channel, we observe the breakup of the beam into filaments, highly localized in a few channels. Of course there is no net amplification of the input beam and power is conserved. In order to form such discrete soliton trains each MI filament collects power from its neighbouring channels. Previous observations of highly localized discrete solitons showed that the power needed to excite essentially a "single channel" soliton in these samples was of the order of 1–2 kW.

Note that the transverse wavevector region over which filamentation occurs extends beyond just $|k_x d| = \pi/2$, as discussed previously and in keeping with the dispersion curves shown in Figs. 4 and 5. This is a consequence of the actual "band structure" found in the AlGaAs arrays, as pointed out by Mandelik *et al*. In fact, the curves obtained in Fig. 9(a) trace out the shape of the fundamental band as a function of $k_x d$.

Excitation with the kind of wide continuous beams used here also excites modes with energy concentrated between the channels, i.e., the second band in our case. The bands effectively overlap around $\Delta\theta = \pi$. From Bloch theory it is known that the curvature of the second band is opposite to that for the first band close to $\Delta\theta = \pi$ and leads to normal diffraction for that case. This is in contrast to the first band for which diffraction is anomalous there as discussed previously. By analogy with the MI theory based on the DNLS (corresponding to the first order band in Bloch theory) the occurrence of filamentation is expected. In the same experiment as described above for the first band, the input beam was tilted beyond the edge of the first Brillouin zone and the beam at the output of the samples was recorded. The results are shown in Fig. 10. As observed in the normal diffraction region of the first band, for low power the beam at the sample output shows a small amount of noise. For increasing input power, the noise becomes amplified. At the highest observed output power the beam breaks into multiple filaments in this second order band.

The dynamic behaviour of a narrower, tilted beam (80 × 1.5 μm FWHM) was also observed. A beam with 80 μm FWHM (corresponding to 9 channels) was used to excite

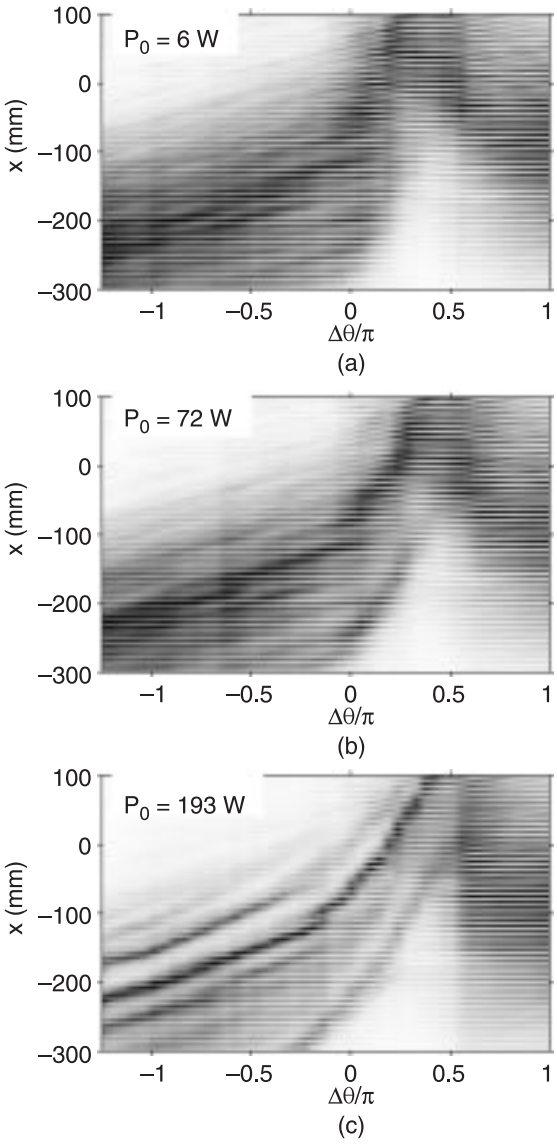

Fig. 10. MI observed in the second band.

an 8 mm long array with a waveguide separation of 9 μm and coupling constant of 800 m^{-1}. The beam was then tilted and the resulting output from the sample was observed. The results are shown in Fig. 11. At low power the beam diffracts and the output position follows the curve expected from Bloch theory. At higher power [Figs. 11(b) and (c)] the beam undergoes discrete self-focusing and localizes in one waveguide at the output. For even higher powers, shown for 1.68 kW in Fig. 11(d), the beam breaks into filaments. This can be explained by the onset of modulational instability (filamentation) for which the period of the filaments varies inversely with input power and the Peierls-Nabarro [25,26] potential responsible for the locking of the beam propagation onto the axial direction of the waveguides.

Corresponding DNLS simulations for a beam tilt of $\Delta\theta = 0.2\pi$ are shown in Fig. 12. Note that the simulations for 900 W predict the onset of beam breakup. The difference from the experimental results can be explained by two

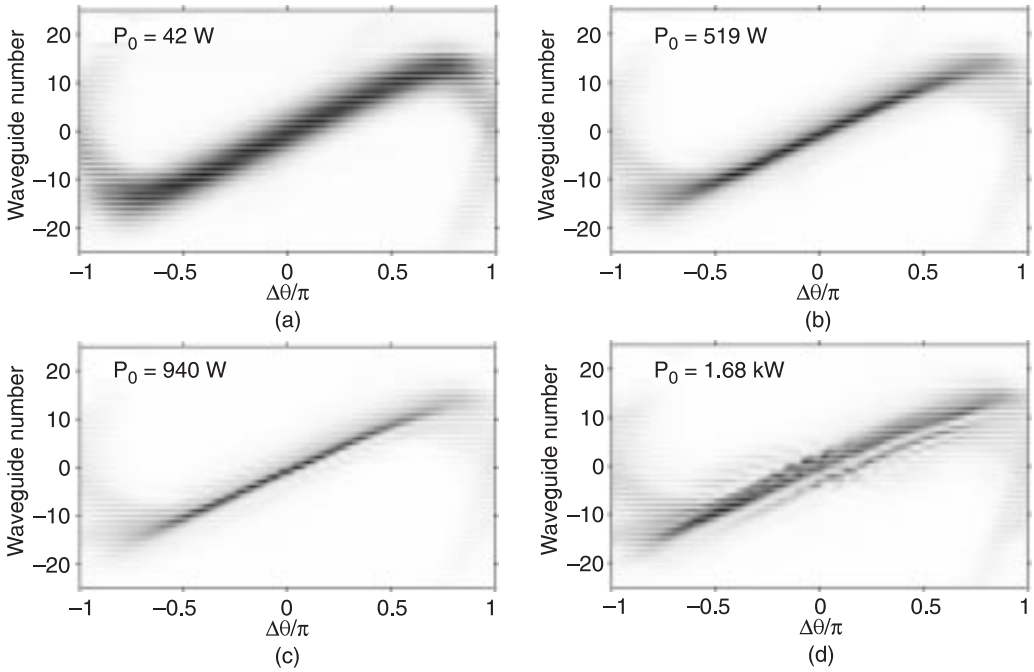

Fig. 11. Output intensity profiles for propagation of a narrow beam with an input power of (a) 42 W, (b) 519 W, (c) 940 W, and (d) 1.68 kW.

factors. First, because the experiment used pulsed excitation and the simulation assumed cw beams, hence the experimental results represent an averaging over the temporal pulse profile. Second, the band shape from the discrete model deviates from the observed one which is better described by the Bloch theory than the DNLS. The locking effect is weaker in the Bloch model.

7. Modulational instability gain

The small signal gain $Im(K_z)$ was measured as a function of input power. This was achieved as discussed previously, namely by crossing two beams inside the array at a variable angle. The growth of the MI is exponential with distance and it quickly saturates in the 8-mm long sample. For the

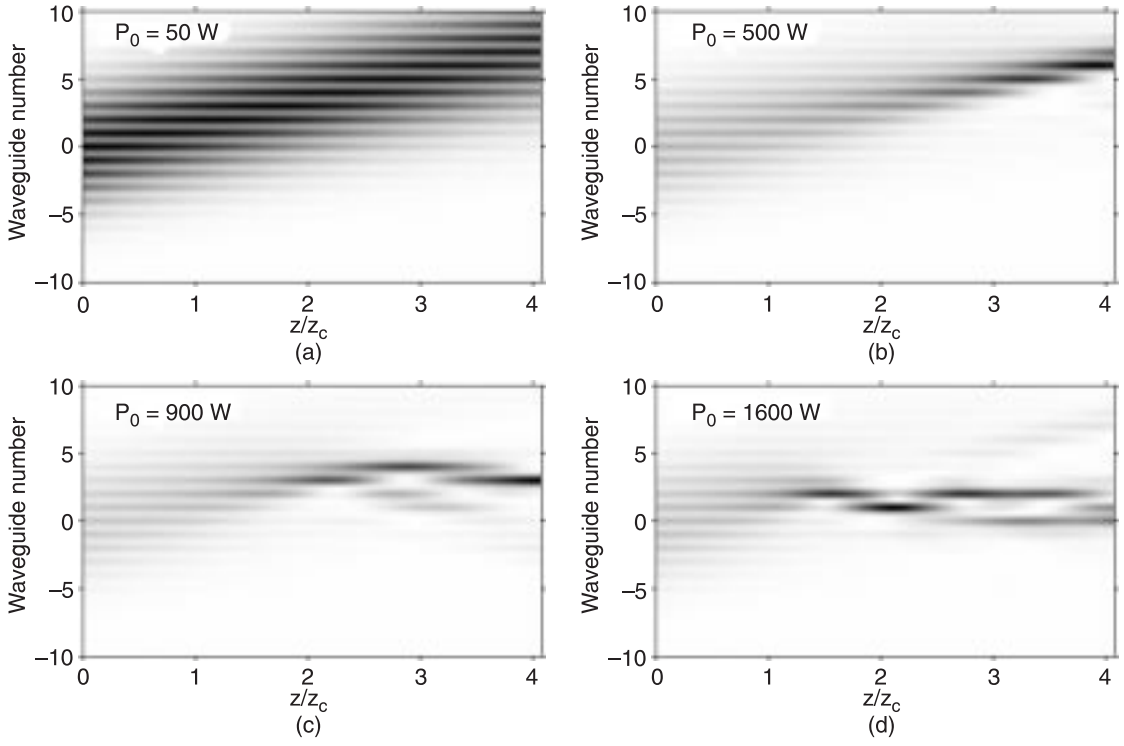

Fig. 12. Coupled mode simulation of the beam propagation for the experiments shown in Fig. 11 with $\Delta\theta = 0.2\pi$ for a input power of (a) 50 W, (b) 500 W, (c) 900 W, and (d) 1600 W.

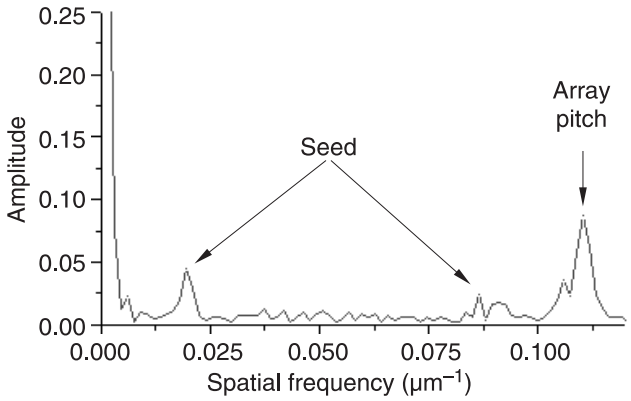

Fig. 13. Fourier transform of the measured output intensity for low power.

gain measurements, the 4-mm long sample with the higher inter-channel coupling constant and smaller propagation length (and hence smaller net gain relative to the 8-mm sample) was used in order to easily measure the power dependence of the gain coefficient. The amplitude of one weak beam is only 5% of the strong beam producing effectively a 10% modulation in the intensity of the strong beam at the input. The interference maxima then grow at the expense of the power between the peaks, increasing effectively the contrast of the interference pattern. The growth rate (K_z) with distance z depends on the period of the interference pattern which determines the value of (K_z). The detailed experimental geometry was shown in Fig. 8.

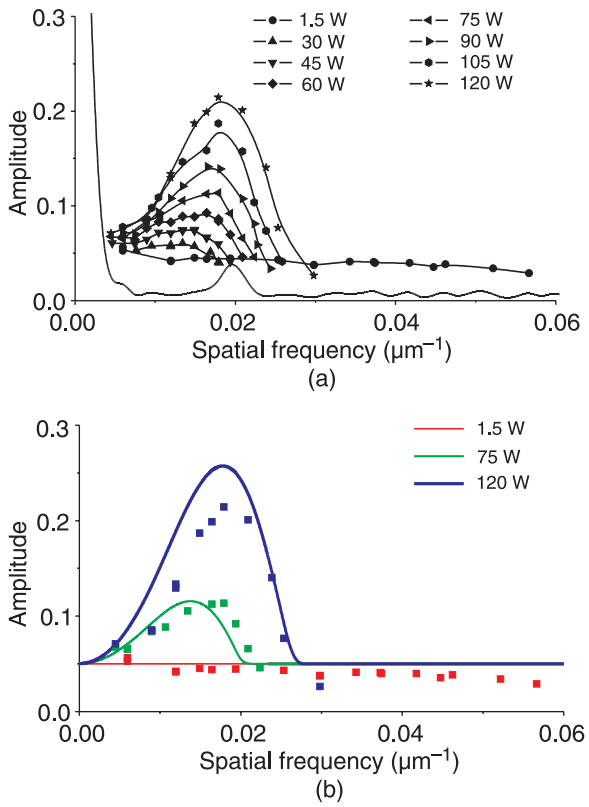

Fig. 14. Measured growth of the first and second spatial harmonic (a). Comparison with theory (b).

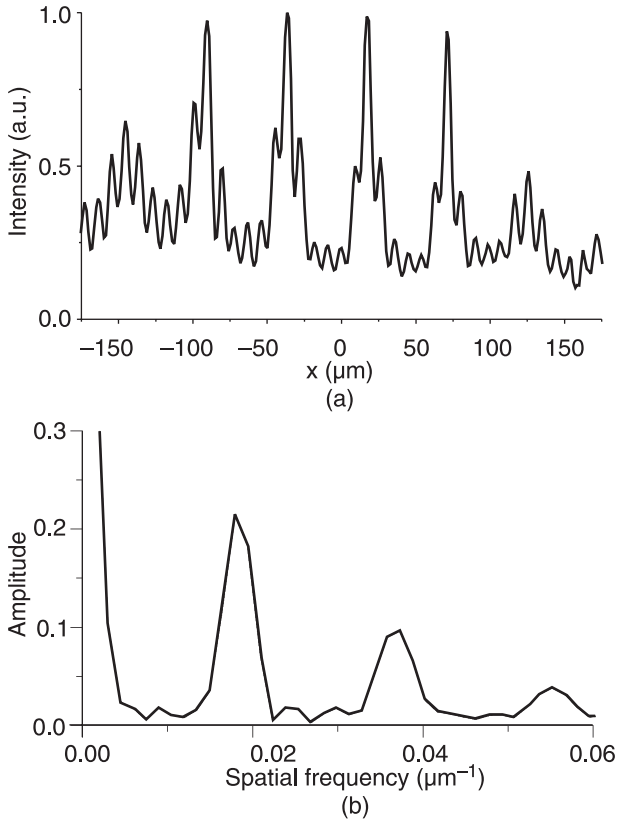

Fig. 15. Filamentation (a) and the corresponding Fourier spectrum (b) for 120 W.

The spatial power distribution at the end of the sample was measured and Fourier transformed. A typical example of the Fourier transform of the intensity pattern obtained at the array output is shown in Fig. 13. Expected and observed were Fourier components at zero spatial frequency and at 0.11 μm^{-1} which correspond to the wide input beam and the modulation due to the channels, respectively. Peaks were also obtained from the periodicity associated with the interference pattern imposed on the incident beam and its "reflection" from the first Brillouin zone of the structure, i.e., the peak at 0.11 μm^{-1}. By varying the relative angle of incidence of the two beams, the periodicity of the interference pattern is changed. The "modulation" peaks moved with the periodicity of the interference pattern. Therefore the increase in the amplitudes and contrast of the fundamental Fourier peaks with increasing input power yields the gain as a function of K_z.

The growth of the modulation instability peaks with increasing input power was measured and is shown in Fig. 14(a). Both the experimental and small signal theory results are shown in Fig. 14(b). At the lowest powers studied (made possible by the sensitivity of the Roper InGaAs array), the pump beam is too weak for the modulation to grow significantly over the length of the sample so that the 5% signal just represents the incident modulation. Growth is first visible with a pump power of 30 W. The gain grows with increasing power, and the maximum shifts over to

larger spatial frequencies. The agreement between experiment and theory is excellent up to a peak channel power of 90 W. At 120 W the measured gain falls well below the theoretical value. The cause is clear from Fig. 15(a) which shows significant generation of higher harmonics, a response well beyond the validity of the small signal gain model described in Sec. 2.

8. Summary

The diverse diffraction properties of arrays have a large impact on the stability of high intensity beam propagation in self-focusing discrete systems. In contrast to homogeneous media in which diffraction is always "normal", there are ranges of directions in discrete systems for which diffraction is "anomalous". In the normal diffraction regions, spatial solitons can exist, and for wide beams filamentation occurs. However, in "anomalous" diffraction regions of propagation, neither bright soliton formation nor filamentation can occur. These conclusions on filamentation were confirmed experimentally for the first time in AlGaAs arrays of channel waveguides in which the nearest-neighbour-channels were coupled via their evanescent field. By operating at photon energies just below half the semiconductor bandgap, an almost ideal Kerr material response was utilized. Although simple coupled mode theory (single band) predicted modulation instability over $|\Delta\theta| < \pi/2$ where $\Delta\theta$ is the phase difference between adjacent channels and no filamentation for $\pi/2 < |\Delta\theta| < \pi$. The actual band structure resulted in filamentation for the range of angles $|\Delta\theta| < 0.6\pi$.

The MI gain was also measured as a function of the spatial periodicity by modulating a strong pump beam (incident at normal incidence onto the array) with a weak seed beam propagating at variable angles to the pump. The input power dependence of the contrast of the interference pattern was measured and found to be in excellent agreement with theory for power ranges over which the small signal theory was valid. At high powers, the saturation of the filamentation led to the generation of higher harmonics of the input interference pattern.

Acknowledgements

This research was supported by an ARO MURI on Gateless Soliton Computing and a BSF joint USA-Israel program.

References

1. D.N. Christodoulides, F. Lederer, and Y. Silberberg, "Discretizing light behaviour in linear and nonlinear waveguide lattices", *Nature* **424**, 817 (2003).
2. S. Somekh, E. Garmire, A. Yariv, H.L. Garvin, and R.G. Hunsperger, "Channel optical waveguide directional couplers", *Appl. Phys. Lett.* **22**, 46 (1973).
3. D.N. Christodoulides and R.I. Joseph, "Discrete self-focusing in nonlinear arrays of coupled wave-guides", *Opt. Lett.* **13**, 794 (1988).
4. A.H. Nayfeh and D.T. Mook, *Nonlinear Oscillations*, Wiley, New York, 1979.
5. E. Enfield and G. Rowlands, *Nonlinear Waves, Solitons, and Chaos*, Cambridge University, Cambridge, 1990.
6. Y.S. Kivshar and G.P. Agrawal, *Optical Solitons: From Fibers to Photonic Crystals*, Academic Press, New York, 2003.
7. G.I. Stegeman and M. Segev, "Optical spatial solitons and their interactions: Universality and diversity", *Science* **286**, 1518 (1999).
8. H. Fang, R. Malendevich, R. Schiek, and G.I. Stegeman, "Spatial modulational instability in one-dimensional lithium niobate slab waveguides", *Opt. Lett.* **25**, 1786 (2000).
9. G.I.A. Stegeman, D.N. Christodoulides, and M. Segev, "Optical spatial solitons: Historical perspectives", *IEEE J. Selected Topics in Quant. Electron.* **6**, 1419 (2000).
10. R. Schiek, H. Fang, R. Malendevich, and G.I. Stegeman, "Measurement of modulational instability gain of second--order nonlinear optical eigenmodes in a one-dimensional system", *Phys. Rev. Lett.* **86**, 4528 (2001).
11. H.S. Eisenberg, Y. Silberberg, R. Morandotti, and J.S. Aitchison, "Diffraction management", *Phys. Rev. Lett.* **85**, 1863 (2000).
12. R. Morandotti, H.S. Eisenberg, Y. Silberberg, M. Sorel, and J.S. Aitchison, "Self-focusing and defocusing in waveguide arrays", *Phys. Rev. Lett.* **86**, 3296 (2001).
13. G.P. Agrawal, *Nonlinear Fiber Optics*, Academic Press, San Diego, 1989.
14. J. Meier, G.I. Stegeman, D.N. Christodoulides, Y. Silberberg, R. Morandotti, H. Yang, G. Salamo, M. Sorel, and J.S. Aitchison, "Experimental observation of discrete modulational instability", *Phys. Rev. Lett.* **92** (2004).
15. A. Yariv, "Coupled-mode theory for guided-wave optics", *IEEE J. Quantum Electron.* **9**, 919 (1973).
16. R.G. Hunsperger, *Integrated Optics: Theory and Technology*, Springer Verlag, Berlin, 2002.
17. A.L. Jones, "Coupling of optical fibers and scattering in fibers", *J. Opt. Soc. Am.* **55**, 261 (1965).
18. H.S. Eisenberg, R. Morandotti, Y. Silberberg, J.M. Arnold, G. Pennelli, and J.S. Aitchison, "Optical discrete solitons in waveguide arrays. I. Soliton formation", *J. Opt. Soc. Am.* **B19**, 2938 (2002).
19. Y.S. Kivshar and M. Peyrard, "Modulational instabilities in discrete lattices", *Phys. Rev.* **A46**, 3198 (1992).
20. K. Alhemyari, A. Villeneuve, J.U. Kang, J.S. Aitchison, C.N. Ironside, and G.I. Stegeman, "Ultrafast all-optical switching in Gaalas directional-couplers at 1.55 Mu-M without multiphoton absorption", *Appl. Phys. Lett.* **63**, 3562 (1993).
21. J.S. Aitchison, A. Villeneuve, and G.I. Stegeman, "Nonlinear directional couplers in AlGaAs", *J. Nonlinear Opt. Phys.* **4**, 871 (1995).
22. J.U. Kang, J.B. Khurgin, C.C. Yang, H.H. Lin, and G.I. Stegeman, "Two-photon transitions between bound-to-continuuan states in AlGaAs/GaAs multiple quantum well", *Appl. Phys. Lett.* **73**, 3638 (1998).
23. J.U. Kang, A. Villeneuve, M. Sheikbahae, G.I. Stegeman, K. Alhemyari, J.S. Aitchison, and C.N. Ironside, "Limitation due to 3-photon absorption on the useful spectral range for nonlinear optics in AlGaAs below half band-gap", *Appl. Phys. Lett.* **65**, 147 (1994).

24. J.S. Aitchison, D.C. Hutchings, J.U. Kang, G.I. Stegeman, and A. Villeneuve, "The nonlinear optical properties of AlGaAs at the half band gap", *IEEE J. Quantum Electron.* **33**, 341 (1997).
25. U. Peschel, R. Morandotti, J.M. Arnold, J.S. Aitchison, H.S. Eisenberg, Y. Silberberg, T. Pertsch, and F. Lederer, "Optical discrete solitons in waveguide array. 2. Dynamic properties", *J. Opt. Soc. Am.* **B19**, 2637 (2002).
26. R. Morandotti, U. Peschel, J.S. Aitchison, H.S. Eisenberg, and Y. Silberberg, "Dynamics of discrete solitons in optical waveguide arrays", *Phys. Rev. Lett.* **83**, 2726 (1999).

